Molecular Electronics

DOI: 10.1002/ange.201105895

Solution-Processed Reduced Graphene Oxide Films as Electronic Contacts for Molecular Monolayer Junctions**

*Sohyeon Seo, Misook Min, Junghyun Lee, Takhee Lee, Sung-Yool Choi, and Hyoyoung Lee**

In monolayer-based molecular electronics, functionalized molecules are utilized as active components; in electronic devices, these functionalities are accessed through stable electrical contacts.[1] In such molecular junctions, a metallic contact can be used to complete a molecular electronic circuit. For practical applications, however, the formation of a soft contact is highly desired to avoid the possibility of a metal filamentary short circuit or molecular damage caused by the penetration of metal atoms into molecular monolayers during direct metal deposition.[2,3] Therefore, contact fabrication techniques such as indirect metal evaporation,[4] surface-diffusion-mediated deposition,[5] and soft organic interlayer coating[6–9] have been developed for molecular electronic devices. One successful technique used for the formation of stable molecular junctions involves the use of a conducting layer of an organic material such as single-walled nanotubes (SWNTs),[9] a conducting polymer (e.g., poly(3,4-ethylenedioxythiophene):poly(4-styrenesulphonic acid), PEDOT:PSS),[6–8] or multilayered graphene[10] as a top electrode or a bridging interfacial layer between the active molecules and a top electrode. These layers can provide proper contact resistance to facilitate true molecular effects in monolayer-based devices composed of alkanethiols/alkanedithiols,[6,10] photoisomers,[8] π-conjugated organic molecules,[9] or metal complexes.[7,11]

Nonetheless, although molecule-dependent electronic transport has been thoroughly investigated, previous interlayer junctions have not allowed for a clear elucidation of the intrinsic properties of functionalized molecules such as memory components in molecular monolayer devices. A reliable device system with a highly sensitive interlayer with molecular functionality is required for the further development of these molecular devices. To develop a highly sensitive interlayer with a high device yield, it is crucial to create an interlayer that is stable, both chemically and electrically, with a soft contact that is able to communicate between the functional molecular monolayer and a metal electrode. To optimize the sensitivity of the interlayer, its thickness should be easily controllable by varying the number of layers. For a stable junction, the interlayer should protect the molecular monolayers from the penetration of hot metal nanoparticles during the vapor deposition of a metallic top electrode because most functional molecular monolayers, which are only a few nanometres thick (< 2–3 nm), are vulnerable to this contamination.

Chemically exfoliated graphene oxide (GO) consists of atomically thin sheets of oxidized graphite that are dispersible in various solvents[12,13] and can be used to produce dispersible reduced graphene oxide (rGO) by chemical reduction.[12] The conductivity of rGO is comparable to that of SWNT[14,15] and is increased by thermal treatment, similar to graphite.[16,17] Graphene and rGO are composed of sp^2 carbon networks and can act as electrodes for electronic devices.[18] One notable advantage of the use of rGO for organic electronics is its solution processability compared with that of graphene. For example, an rGO film electrode can be easily prepared by spin-coating an rGO solution[19] onto a substrate or by spin-coating with GO followed by vapor reduction.[20] Additionally, the strong π–π interactions between rGO nanosheets result in a graphite interlayer distance of approximately 0.34 nm, leading to a high conductivity that is comparable to that of highly oriented pyrolytic graphite (HOPG).[20] Electrical conduction in rGO thin films is treated as that through a semimetal such as graphite, and the contact resistance in rGO devices is negligible.[21] Because rGO has high chemical stability, mechanical strength, and a work function comparable to that of gold,[22] rGO has been considered to be a promising candidate for interfacial electronic contacts in monolayer molecular electronics.

Herein, we report the development of a solution-processed electronic contact between rGO thin films and molecular components in monolayer-based devices. The rGO contact allows for stable monolayer junctions of alkanethiol monolayers (e.g., molecular resistors) and redox-active metal complex monolayers[23] (e.g., molecular memories) that prevent the formation of metallic short circuits and exhibit excellent junction preservation. The effects of monolayer thickness and molecular functionality were examined in novel molecular junctions using rGO interlayers. Through the semimetallic rGO interlayer contact, the current hysteresis loops and threshold conductance

[*] Dr. S. Seo, M. Min, Dr. J. Lee, Dr. H. Lee
National Creative Research Initiative, Center for Smart Molecular Memory, Department of Chemistry, Samsung-SKKU Graphene Center, Sungkyunkwan University
300 Cheoncheon-dong, Jangan-gu, Suwon, Gyeonggi-do 440-746 (Korea)
E-mail: hyoyoung@skku.edu
Dr. T. Lee
Department of Materials Science and Engineering, Gwangju Institute of Science and Technology
Gwangju (Korea)
Dr. S.-Y. Choi
Electronics and Telecommunications Research Institute (ETRI)
Daejeon (Korea)

[**] This work was supported by the Creative Research Initiatives (project title: Smart Molecular Memory) of MEST/NRF.

Supporting information for this article including material synthesis and characterization is available on the WWW under http://dx.doi.org/10.1002/anie.201105895.

 © 2012 Wiley-VCH Verlag GmbH & Co. KGaA, Weinheim

voltages of a redox-active metal complex monolayer were measured in a new molecular contact system, showing true molecular effects that depend on molecular redox properties.

Solvent-dispersed rGO sheets were produced by the reduction of GO sheets dispersed in water using a reaction mixture of hydrazine and aqueous ammonia (Figure S1; see Supporting Information for synthesis and characterization). The conductivity of the synthesized rGO film (with thickness of 6.5 ± 0.5 μm) was approximately 7600 ± 200 S m^{-1},[14] thus indicating the production of rGO sheets with much higher conductivities than that of highly doped PEDOT:PSS.[6]

Schematic diagrams of the fabrication processes for monolayer-based devices using rGO interlayers are presented in Figure 1. Well-dispersed rGO sheets in solution were spin-coated onto an Au bottom electrode. An Au top electrode was vapor-deposited on the rGO film (to approximately 10 nm thickness) at a low deposition rate of 0.1 Å s^{-1}. No hysteresis or metallic filamentary conductance was observed in the current–voltage (I/V) curves, hence indicating that the rGO interlayer successfully prevented the penetration of top-metal particles (Figure 1 a). The low-bias resistance was determined to be 160 ± 5 Ω (at 1.0 V with 95 % confidence), as measured in 20 devices (> 99 % yield).

The contact effects of the rGO interlayer in molecular electronic devices were examined in monolayer-based junctions. Self-assembled monolayers (SAMs) of alkanethiols (e.g., 1-octanethiol (C8), 1-decanethiol (C10), and 1-dodecanethiol (C12)) behaved as molecular resistors in the molecular junctions (Figure 1 b). The resistance of the C10 SAM device was 4500 ± 50 Ω (at 1.0 V with 95 % confidence), as measured in 50 devices (> 99 % yield). Furthermore, the SAMs of bis-thiophenylterpyridine-transition metal(II) complexes ($[M_T^{II}(tpyphs)_2]$, where $M_T^{II} = Fe^{II}$, Ru^{II}, or Co^{II}) behaved as molecular memories in the molecular junctions (Figure 1 c). The I/V curves of the Au/rGO film/$[Co^{II}(tpyphs)_2]$ monolayer/Au device showed sharp conductance switching and large hysteresis loops. A cross-section of the functionalized monolayer-based devices showed that the rGO interlayer protected the SAM well (Figure S2).

Figure 2 shows the evaluation of the electron transport behaviors of the molecular junctions of three alkanethiol SAMs. In Figure 2 a, current density is plotted on a logarithmic scale as a function of applied voltage for the alkanethiol monolayers; the error bars represent the standard deviation and corresponding average values (with 95 % confidence) for 50 devices. Current density was observed to decrease as the molecular length of the alkanethiols was increased. The current density of the alkanethiol monolayer junctions was exponentially dependent on the molecular length, thus indicating that the dominant conductance mechanism was tunnelling.[24,25] The I/V characteristics shown in Figure 2 b indicate that the three alkanethiol devices exhibited no noticeable degradation after storage under vacuum conditions for 30 days. Figure 2 c presents current density plots at several biases as a function of molecular length. The current density (J) plot as a function of the barrier width (d) can be described by the expression $J \propto \exp(-\beta d)$, where β is the tunneling decay coefficient. Here, the average value of β was 0.82 ± 0.12 Å^{-1}, which is in agreement with previously reported values for alkanethiol junctions.[10,26,27] This result confirms that the new rGO interlayer device system operates reliably to give molecular transport properties through monolayer junctions.

The molecular conductance states that mediate electron transport in the molecular electronic devices were determined from their I/V characteristics such as the threshold voltage for conductance switching. The redox potentials of electrochemically active molecules

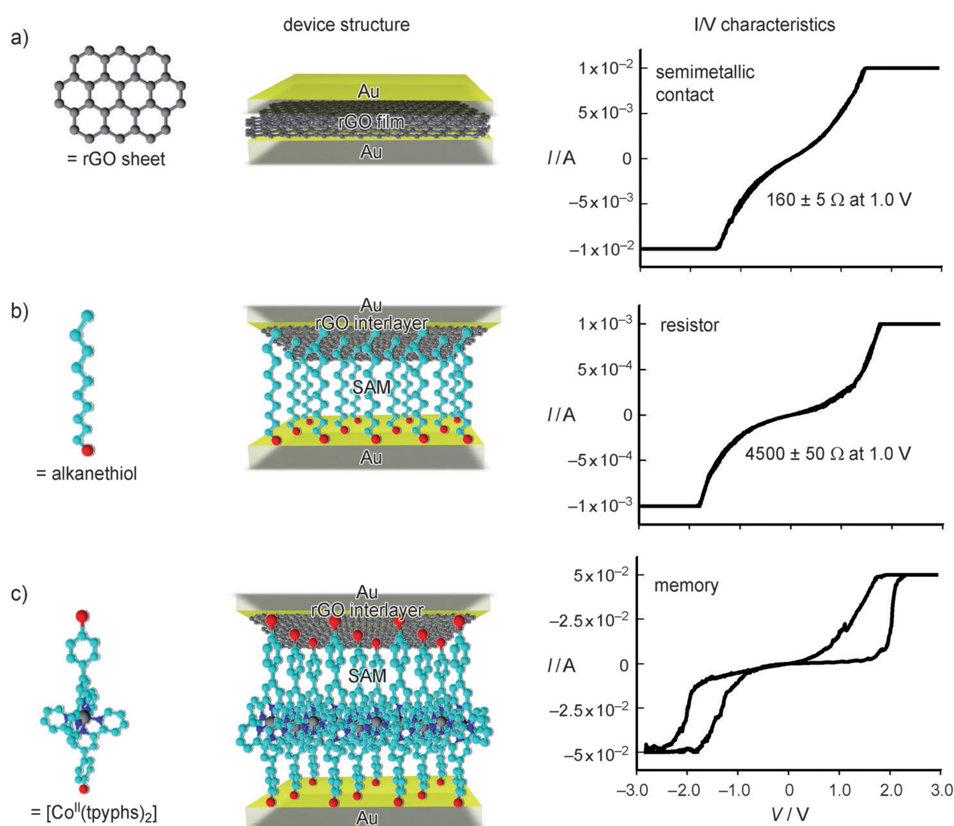

Figure 1. Fabrication of a soft electronic contact for monolayer-based molecular devices. a) An Au/rGO film/Au junction and its current–voltage (I/V) characteristics, exhibiting low resistance. b), c) Au/rGO film/molecular monolayer/Au junctions and I/V characteristics. The alkanethiol self-assembled monolayer (SAM) in (b) shows high resistance, and the metal complex SAM in (c) shows hysteretic conductance switching.

 © 2012 Wiley-VCH Verlag GmbH & Co. KGaA, Weinheim

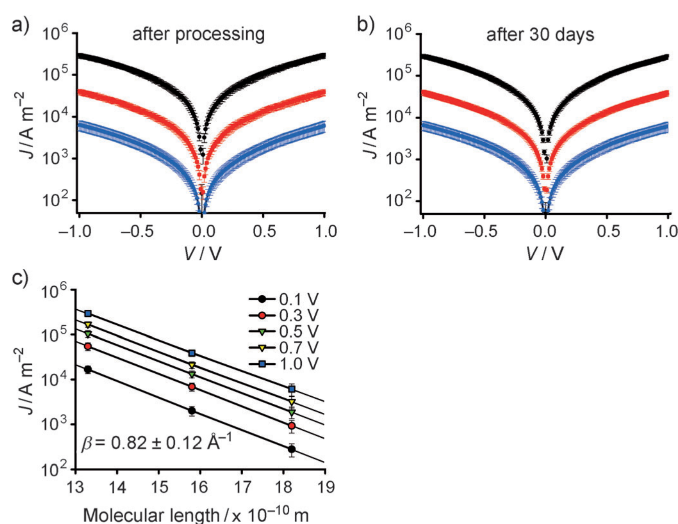

Figure 2. Effects of monolayer thickness on new molecular junctions with an rGO interlayer. a), b) Current density–voltage profiles plotted on a log scale for alkanethiol monolayers in rGO interlayer junctions after processing (a) and after 30 days of storage (b). Alkanethiol SAMs are 1-octanethiol (C8, black), 1-decanethiol (C10, red), and 1-dodecanethiol (C12, blue). c) Plots of current densities at different voltages versus the molecular lengths of the alkanethiol SAMs from the plots in (a).

are intrinsic characteristics, and electron transport in these molecules occurs across their molecular redox states when the molecules are placed between two electrodes.[28] However, the interlayers establishing electronic contact in monolayer-based electronic devices may or may not be sensitive to conductance switching at the molecular level due to the redox reaction potential. Thus, the precise mechanism for the current hysteresis observed as a function of conductance switching in redox-active monolayer junctions has not yet been elucidated. As a characteristic aspect of the conductance switching of redox-active monolayers, the molecular charging energy involves the electrochemical potential of a molecular conducting state.[28] A redox-active transition metal(II) complex has discrete redox states that are induced by the coordination of a conjugated ligand to a metal center, which produces metal-center-dependent redox reaction potentials in the associated cyclic voltammograms (CVs; Figure 3a). The formal redox potentials measured with respect to M^{III}/M^{II} redox couples were measured against a saturated calomel electrode (SCE) as reference and converted to vacuum levels; $V_{abs}(eV) = 4.7\,eV + E^0(SCE)$,[28] where E^0 is the formal redox potential and 4.7 eV was approximated based on the vacuum level of the SCE reference electrode. Furthermore, the electronic transition between molecular redox states that appears at 450–650 nm caused by metal-to-ligand charge transfer (MLCT) is related to the energy gap between the highest occupied molecular orbital (HOMO) and the lowest unoccupied orbital (LUMO; Figure 3b). The HOMO–LUMO gap energies were calculated using the absorption energies calculated by the extrapolation of the MLCT peaks. Consequently, the redox molecular states (e.g., HOMO and LUMO) of the $[M_T^{II}(tpyphs)_2]$ monolayer were available from the electrochemical measurements and the UV/Vis absorption measurements shown in Figure 3.

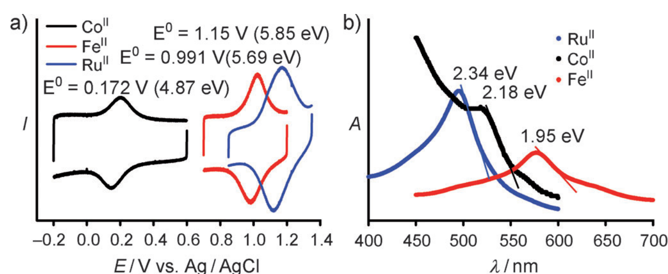

Figure 3. Characterization of redox-active molecular monolayers. a) Solid-state cyclic voltammograms (CVs) of $[M^{II}(tpyphs)_2]$ SAMs on ITO substrates in $HClO_4$ (0.1 M) at a scan rate of 0.1 $V\,s^{-1}$; b) solid-state UV/Vis spectra of $[M^{II}(tpyphs)_2]$ films on ITO substrates.

On the other hand, redox-active molecular monolayers showed unique *I*/*V* characteristics when incorporated into a novel electronic contact system. Figure 4a–c shows representative *I*/*V* curves on a linear scale for each Au/rGO film/$[M_T^{II}(tpyphs)_2]$ monolayer/Au junction exhibiting conductance switching between low-conducting and high-conducting states. The threshold conductance voltages in

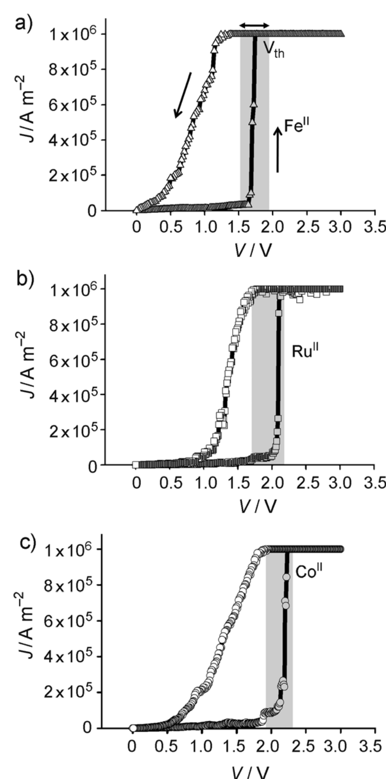

Figure 4. Effects of molecular functionality in new molecular junctions with an rGO interlayer. *I*/*V* characteristics on a linear scale for Au/rGO film/$[M_T^{II}(tpyphs)_2]$ monolayer/Au junctions show conductance switching at approximately 1.75 V for $[Fe^{II}(tpyphs)_2]$ (a), at approximately 2.05 V for $[Ru^{II}(tpyphs)_2]$ (b), and at approximately 2.20 V for $[Co^{II}(tpyphs)_2]$ (c). The threshold conductance voltages observed in each molecular junction from 50 devices are indicated as V_{th} in each *I*/*V* curve.

© 2012 Wiley-VCH Verlag GmbH & Co. KGaA, Weinheim

the $[M_T^{II}(tpyphs)_2]$ monolayer devices were dependent on the central metal atoms of $[M_T^{II}(tpyphs)_2]$ (e.g., 1.5–1.9 V for $[Fe^{II}(tpyphs)_2]$, 1.7–2.1 V for $[Ru^{II}(tpyphs)_2]$, and 1.9–2.3 V for $[Co^{II}(tpyphs)_2]$, which were measured in 50 devices for each complex). The conductance switching behavior of these molecules is a consequence of molecular resonant tunneling due to the energetic alignment of the molecular state with the Fermi level of the metal at a specific voltage. The current hysteresis loop also resulted from the switching between two states, with electron charge involving the electrochemical reaction of the redox-active molecules. Thus, the molecular charging energy at the high-conducting state corresponds to the energy difference between the electrochemical potential of the redox-active molecules and the Fermi level of the metal. The threshold conductance voltages of each $[M_T^{II}(tpyphs)_2]$ are in good agreement with the energy gaps between the Au Fermi level and the electron affinity level of each metal complex. The electron affinity level (i.e., LUMO) of the metal complexes was obtained from the ionization energy (i.e., HOMO) and the MLCT electronic transition energy (i.e., the HOMO–LUMO gap). From the CV data shown in Figure 3a, the formal redox potentials (i.e., the ionization potentials corresponding to the HOMO) of these complexes were determined to be 5.69 eV, 5.85 eV, and 4.87 eV below vacuum for $[Fe^{II}(tpyphs)_2]$, $[Ru^{II}(tpyphs)_2]$, and $[Co^{II}(tpyphs)_2]$ respectively. As determined from the UV/Vis absorption spectra (Figure 3b), the HOMO–LUMO energy gaps for the complexes were 1.95 eV, 2.34 eV, and 2.18 eV for $[Fe^{II}(tpyphs)_2]$, $[Ru^{II}(tpyphs)_2]$, and $[Co^{II}(tpyphs)_2]$ respectively. The corresponding LUMO levels of the complexes were then calculated to be 3.74 eV, 3.51 eV, and 2.93 eV below vacuum for $[Fe^{II}(tpyphs)_2]$, $[Ru^{II}(tpyphs)_2]$, and $[Co^{II}(tpyphs)_2]$, respectively. Therefore, the theoretical threshold conductance voltages were determined by the energy gap between the metal Fermi level (5.1–5.3 eV for Au)[23,28,29] and each LUMO level; the average values were approximately 1.7 ± 0.2 eV, 1.8 ± 0.2 eV, and 2.2 ± 0.2 eV for $[Fe^{II}(tpyphs)_2]$, $[Ru^{II}(tpyphs)_2]$, and $[Co^{II}(tpyphs)_2]$. These calculated values agree well with the experimental values (see Figure 4a–c).

To demonstrate the performance of a molecular memory component in the rGO interlayer junctions, memory reversibility tests for the Au/rGO film/$[M_T^{II}(tpyphs)_2]$ monolayer/Au junction were examined by write/multiple read/erase/multiple read (WRER) operations[7,9] (Figure 5). At 1.5 V, representing an intermediate reading voltage, the ON/OFF current ratio for the high-conducting state (ON) and the low-conducting state (OFF) of $[M_T^{II}(tpyphs)_2]$ monolayers was shown to be approximately five. Such small ON/OFF ratios have often been observed in monolayer-based memory devices containing redox-active molecules,[7,9] whereas large ON/OFF ratios have been reported in spin-coated thick films.[30,31] As film thickness is increased, the OFF current sharply decreases, leading to an increased ON/OFF ratio.[31] Thus, molecular monolayers that are a few nanometers thick (< 2–3 nm) are expected to lead to small ON/OFF ratios. Although large ratios are advantageous, they are not always required for potential applications,[32] especially in very thin

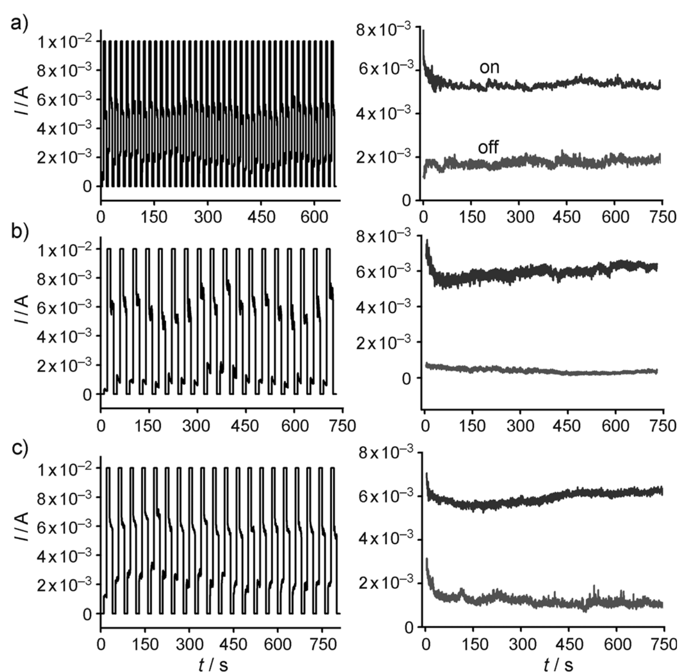

Figure 5. Memory effect of Au/rGO film/$[M_T^{II}(tpyphs)_2]$ monolayer/Au devices. Write/multiple read/erase/multiple read operations are shown in the left panel and the corresponding ON and OFF retentions are shown in the right panel for molecular monolayers of $[Ru^{II}(tpyphs)_2]$ (a), $[Fe^{II}(tpyphs)_2]$ (b), and $[Co^{II}(tpyphs)_2]$ (c).

layers. The write/erase operations were also achieved by continuous reading at + 1.5 V after pulsing voltages for 1.5 s at + 3.0 V for the ON state and 0.0 V for the OFF state. WRER cycles for a $[Ru^{II}(tpyphs)_2]$ device were conducted over 40 times (Figure 5a) for one test set, and good reproducibility was observed in the following five test sets. The memory effects of $[Fe^{II}(tpyphs)_2]$- and $[Co^{II}(tpyphs)_2]$-monolayer-based rGO junctions were also successfully programmed (Figure 5b for $[Fe^{II}(tpyphs)_2]$ and Figure 5c for $[Co^{II}(tpyphs)_2]$). The retention time of each ON and OFF state in all of the memory devices was sustained for a minimum of 10 min, which is characteristic of nonvolatile memory.

In conclusion, solution-processed rGO films were demonstrated as universal electronic contacts that can be used to elucidate the electronic functionality of molecular resistors or molecular memories in molecular electronic devices. Due to the semimetallic property of rGO thin films, they exhibit high conductivity; the rGO-interlayer contact showed interesting electronic characteristics comparable to those of a metallic contact system such as gold nanoparticle and nanowire contacts. The rGO electronic contact represents a new test bed for solution-processable and universal applications of monolayer-based molecular devices with high sensitivity because of its molecular functionality and high device yield.

Experimental Section

Fabrication of rGO-interlayer devices with SAMs: The synthesized rGO was dissolved in DMF ($0.5\ mg\,mL^{-1}$). The supernatant of the rGO solution was used for spin-coating to produce an rGO film on an

© 2012 Wiley-VCH Verlag GmbH & Co. KGaA, Weinheim

Au electrode for monolayer molecular devices. Au bottom electrodes (80 nm thick) were deposited on Ti (5 nm)/SiO_2 (300 nm)/Si by electron-beam evaporation at a low deposition rate (0.1 Å s^{-1}). [M_T^{II}(tpyphs)$_2$] (3 mM; see Supporting Information for synthesis) in DMF was used to produce a SAM on the Au bottom electrodes by a 36 h immersion after deprotection of the thioacetate groups by adding approximately 15 µL of aqueous ammonia (28 wt%, Aldrich). SAMs of alkanethiols (e.g., C8, C10, and C12, all purchased from Aldrich) were prepared by immersing the Au substrate in 2 mM alkanethiol in ethanol for 24 h. All substrates were prepared by chemical cleaning using piranha solution (H_2SO_4:H_2O_2 at 3:1, a very strong oxidant requiring caution in handling), washing with deionized water and ethanol, and drying with N_2 gas. The well-dispersed rGO sheets in solution were spin-coated onto the SAMs, and Au top electrodes (100 × 100 μm^2) 60 nm thick were then vapor-deposited (0.1 Å s^{-1}) on the rGO film/SAM/Au bottom electrodes. The electrical characteristics of the devices were measured by a Keithley 4200-SCS semiconductor characterization system in vacuum.

Received: August 20, 2011
Published online: November 11, 2011

Keywords: molecular electronics · molecular monolayer junctions · nanotechnology · reduced graphene oxide · self-assembly

[1] R. L. McCreery, *Chem. Mater.* **2004**, *16*, 4477–4496.
[2] G. L. Fisher, A. V. Walker, A. E. Hooper, T. B. Tighe, K. B. Bahnck, H. T. Skriba, M. D. Reinard, B. C. Haynie, R. L. Opila, N. Winograd, D. L. Allara, *J. Am. Chem. Soc.* **2002**, *124*, 5528–5541.
[3] A. V. Walker, T. B. Tighe, O. M. Cabarcos, M. D. Reinard, B. C. Haynie, S. Uppili, N. Winograd, D. L. Allara, *J. Am. Chem. Soc.* **2004**, *126*, 3954–3963.
[4] H. Haick, M. Ambrico, J. Ghabboun, T. Ligonzo, D. Cahen, *Phys. Chem. Chem. Phys.* **2004**, *6*, 4538–4541.
[5] A. P. Bonifas, R. L. McCreery, *Nat. Nanotechnol.* **2010**, *5*, 612–617.
[6] H. B. Akkerman, P. W. M. Blom, D. M. de Leeuw, B. de Boer, *Nature* **2006**, *441*, 69–72.
[7] J. Lee, H. Chang, S. Kim, G. S. Bang, H. Lee, *Angew. Chem.* **2009**, *121*, 8653–8656; *Angew. Chem. Int. Ed.* **2009**, *121*, 8501–8504.
[8] A. J. Kronemeijer, H. B. Akkerman, T. Kudernac, B. J. Van Wees, B. L. Feringa, P. W. M. Blom, B. De Boer, *Adv. Mater.* **2008**, *20*, 1467–1473.
[9] J. He, B. Chen, A. K. Flatt, J. J. Stephenson, C. D. Doyle, J. M. Tour, *Nat. Mater.* **2006**, *5*, 63–68.
[10] G. Wang, Y. Kim, M. Choe, T. W. Kim, T. Lee, *Adv. Mater.* **2011**, *23*, 755–760.
[11] Z. Ng, K. P. Loh, L. Li, P. Ho, P. Bai, J. H. K. Yip, *ACS Nano* **2009**, *3*, 2103–2114.
[12] S. Park, J. An, I. Jung, R. D. Piner, S. J. An, X. Li, A. Velamakanni, R. S. Ruoff, *Nano Lett.* **2009**, *9*, 1593–1597.
[13] Y. Zhu, S. Murali, W. Cai, X. Li, J. W. Suk, J. R. Potts, R. S. Ruoff, *Adv. Mater.* **2010**, *22*, 3906–3924.
[14] D. Li, M. B. Müller, S. Gilje, R. B. Kaner, G. G. Wallace, *Nat. Nanotechnol.* **2008**, *3*, 101–105.
[15] V. Skákalová, A. B. Kaiser, U. Dettlaff-Weglikowska, K. Hrncarikova, S. Roth, *J. Phys. Chem. B* **2005**, *109*, 7174–7181.
[16] G. Eda, M. Chhowalla, *Adv. Mater.* **2010**, *22*, 2392–2415.
[17] C. Mattevi, G. Eda, S. Agnoli, S. Miller, K. A. Mkhoyan, O. Celik, D. Mastrogiovanni, C. Cranozzi, E. Carfunkel, M. Chhowalla, *Adv. Funct. Mater.* **2009**, *19*, 2577–2583.
[18] P. H. Wöbkenberg, G. Eda, D. S. Leem, J. C. De Mello, D. D. C. Bradley, M. Chhowalla, T. D. Anthopoulos, *Adv. Mater.* **2011**, *23*, 1558–1562.
[19] G. Eda, M. Chhowalla, *Nano Lett.* **2009**, *9*, 814–818.
[20] I. K. Moon, J. Lee, R. S. Ruoff, H. Lee, *Nat. Commun.* **2010**, DOI: 10.1038/ncomms1067.
[21] G. Eda, C. Mattevi, H. Yamaguchi, H. Kim, M. Chhowalla, *J. Phys. Chem. C* **2009**, *113*, 15768–15771.
[22] S. Pang, H. N. Tsao, X. Feng, K. Mullen, *Adv. Mater.* **2009**, *21*, 3488–3491.
[23] K. Seo, A. V. Konchenko, J. Lee, G. S. Bang, H. Lee, *J. Am. Chem. Soc.* **2008**, *130*, 2553–2559.
[24] R. E. Holmlin, R. Haag, M. L. Chabinyc, R. F. Ismagilov, A. E. Cohen, A. Terfort, M. A. Rampi, G. M. Whitesides, *J. Am. Chem. Soc.* **2001**, *123*, 5075–5085.
[25] W. Wang, T. Lee, M. A. Reed, *Phys. Rev. B* **2003**, *68*, 354161.
[26] V. B. Engelkes, J. M. Beebe, C. D. Frisbie, *J. Am. Chem. Soc.* **2004**, *126*, 14287–14296.
[27] B. Q. Xu, N. J. J. Tao, *Science* **2003**, *301*, 1221–1223.
[28] J. He, Q. Fu, S. Lindsay, J. W. Ciszek, J. M. Tour, *J. Am. Chem. Soc.* **2006**, *128*, 14828–14835.
[29] A. K. Mahapatro, J. Ying, T. Ren, D. B. Janes, *Nano Lett.* **2008**, *8*, 2131–2136.
[30] B. Pradhan, S. Das, *Chem. Mater.* **2008**, *20*, 1209–1211.
[31] J. Lee, E. Lee, S. Kim, G. S. Bang, D. A. Shultz, R. D. Schmidt, M. D. E. Forbes, H. Lee, *Angew. Chem.* **2011**, *123*, 4506–4510; *Angew. Chem. Int. Ed.* **2011**, *50*, 4414–4418.
[32] H. J. Kim, W. C. Jeong, K. H. Koh, G. T. Jeong, J. H. Park, S. Y. Lee, J. H. Oh, I. H. Song, H. S. Jeong, K. Kim, *IEEE Trans. Magn.* **2003**, *39*, 2851–2853.

 © 2012 Wiley-VCH Verlag GmbH & Co. KGaA, Weinheim